

# Simulation and Comparison of Helical and Straight-Bladed Hydrokinetic Turbines

Mohammad A. AL-DABBAGH\*, Mehmet Ishak YUCE \*\*‡

\*Northern Technical University NTU, Technical Institute/ Mosul, department of water resources techniques, Mosul, Iraq.  
+9647738289044

\*\* University of Gaziantep, Turkey, +90 507 702 0560

(mohamed.akram@ntu.edu.iq, yuce@gantep.edu.tr)

‡ Corresponding Author; Mehmet Ishak YUCE, Civil Engineering Department, University of Gaziantep, +90 507 702 0560,  
yuce@gantep.edu.tr

*Received: 13.06.2017 Accepted: 07.08.2017*

**Abstract-** In this article simulation analyses have been performed using computational fluid dynamics techniques to investigate the performance of helical and straight-bladed cross flow hydrokinetic turbines with a horizontal layout and similar dimensions. The length and diameter and the type of the hydrofoil of both turbines are selected to be the same. A symmetrical NACA hydrofoil has been used in blade design for both turbines. The simulation analyses were performed for a 2-D NACA0018 hydrofoil and 3-D four bladed turbines. The skewness coefficient and the orthogonal quality tests have been dependent as statistical tools to examine the quality of the mesh for all models. The obtained results have shown that the helical turbine reaches the stall condition at the tip-speed ratio (TSR) of 3.75, while the straight-bladed turbine stops converting energy at 3.1. The highest power coefficient for the helical turbine was about 0.37, while it was found to be around 0.29 for the straight-bladed turbine. These results demonstrate that a helical turbine of 1.5 m in length and 1 m in diameter is more efficient than the same-sized straight-bladed turbine under the same flow conditions.

**Keywords-** Hydrokinetic Turbines; Helical Turbines; Straight-bladed Turbines; Power Coefficient; CFD.

## 1. Introduction

Water currents are the largest source of clean, renewable energy, which represents an enormous amount of energy in different forms such as ocean waves and marine currents [1]. Recently, due to the increasing demand for power generation, the scientific ideas are tended toward other alternatives in order to get power with less time and low initial cost and at the same time be eco-friendly [2 – 8]. Water power is a significant source of renewable energy, where the waters represent 70% of the earth's surface and considered as an enormous source of energy in the form of wave, tidal and marine current [9, 10]. Although, utilization of the conventional hydro-turbines are proven to be very efficient in high-head flows, they are unsuccessful and expensive in low-head and ultra-low-head applications [11, 12]. In low-head hydroelectric power stations, the cost of Kaplan, Francis and Pelton turbines, which are the most widely, skyrockets when they are used for low-heads from 5 to 2 m [13].

Flowing waters such as, ocean currents, tidal flows and river streams contain a huge amount of kinetic energy, which

could be harnessed by hydrokinetic turbines. Nonetheless, this resource has not yet been efficiently exploited [14, 15]. The exploitation of the energy of the flowing water by employing a turbine is very similar to the application of wind turbines, which is considered as a fledgling form of renewable energy compared to wind energy [4, 16 – 18]. In-stream technology concept includes converting the kinetic energy of the flowing water caused by tides and earth's gravitational force (open-channel flow), into electricity. Generally, this technology includes submerged or partially submerged hydrokinetic turbines. Moreover, in-stream conversion devices are less influenced by weather unlike other renewable technologies, such as wind, wave and solar energy systems [1]. Tidal flow depends on moon gravity relative to the earth, while flowing water is subject to the gravity and difference in head. These topics were the focus of many researchers [19] where Gorlov (1998) [13] investigated the performance of the vertical 3-bladed helical turbine using NACA0020 with about 18 cm chord length. His model demonstrated a quite good performance with power coefficient of about 35% at water velocity of  $1.5 \text{ m s}^{-1}$ .

Moreover, McAdam (2011) [20] studied experimentally and analytically the helical turbines, where the author used different solidities with different numbers of blades and the designed turbine attained efficiency of 24% at a flow velocity of  $0.8 \text{ m s}^{-1}$ . Meanwhile, Yang et al. (2012) [21] designed a new hydrofoil for a helical turbine placed vertically to convert the water currents to energy. Recently, Gebreslassie et al. (2013) [22] studied the interaction between the turbines, where the simulation results have shown that the lateral space is affecting on the turbine performance. The helical and straight-bladed turbines are two well-known types of hydrokinetic turbines, which are considered as cross-flow devices. The straight-bladed turbine was developed in 1920 by G. J. Darrieus [23], Fig.1 a. It is characterized by straight blades of hydrofoil-shape and is considered as a lift cross flow turbine operating with high TSRs compared with drag devices such as Savonius rotor. On the other hand, the helical turbine was developed in 1995 by A. Gorlov (1998), Fig.1b. The general concept of the helical turbine is similar to the straight-bladed turbine, except that its blades have a helical path unlike the straight blades the straight-bladed turbine has. In the present study, numerical analyses were conducted by using ANSYS FLUENT software in order to determine the performance of the same size straight-bladed and helical cross flow hydrokinetic turbines, 1.5 m in length and 1 m in diameter, under the same flow conditions.

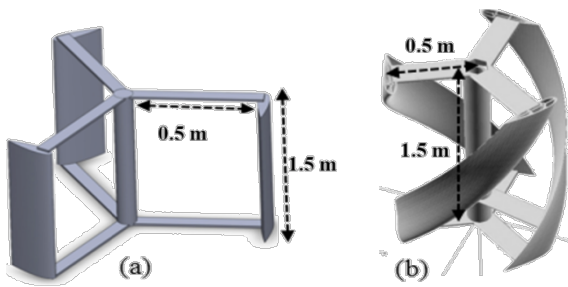


Fig. 1. (a) Straight-bladed turbine, (b) Helical turbine

## 2. The Non-dimensional Constraint Parameters

To use a hydrokinetic turbine to convert energy, the dynamics of the turbine must be fully understood. Usually, different governing parameters are controlling the hydrokinetic devices.

The hydro-dynamic aspects of hydrokinetic turbine design that directly impact the energy conversion are the Reynolds number, tip-speed ratio, solidity and efficiency. The angular speed of the turbine is a function of the water flow velocity. Since the turbines studied in the present article are classified as stall regulated, when the angular velocity is increased further than the cut-off speed of the turbine, its efficiency is expected to be reduced. That is why, the change in the angular velocity becomes more important to be considered to examine the performance of the turbine. The tip speed ratio (TSR) is the speed of the blade's tip ( $\Omega R$ ) divided by the flow velocity [24] Therefore, different TSRs are considered in the present study for a single Reynolds number [25 – 28].

$$\lambda = \frac{\Omega R}{v_\infty} \quad (1)$$

Where  $\lambda$  is the TSR,  $R$  is the radius of the sweeping area of the turbine (m),  $\Omega$  is the turbine's rotational velocity ( $\text{rad s}^{-1}$ ),  $v_\infty$  is free stream velocity ( $\text{m s}^{-1}$ ).

The tangential velocity of the tip of the blade ( $\omega R$ ) signifies the magnitude of the torque to be created. Gorlov (1998) observed that TSR range at the maximum torque created on a 3-bladed helical turbine is about 2.0 to 2.2 in order to avoid cavitation. A Savonius rotor generates the optimum lift when  $\lambda \leq 1$  [29]. The lift device that includes a hydrofoil section usually, operates at tip-speed ratios above unity. In straight-bladed Darrieus turbines, lower tip-speed ratio makes the angle of attack of the hydrofoil to reach much higher levels than other cross-flow hydrokinetic turbines [27, 30, 31 and 32]. Meanwhile, a high TSR does not mean a high power coefficient ( $C_p$ ). Al-Sam (2010) [33] observed that at a fixed geometry and fixed inlet conditions, the efficiency of a water wheel turbine (or the power coefficient) increases as the TSR increases until a certain point where its efficiency is maximum and then it gradually starts to decrease as the tip-speed ratio is increased further [34].

## 3. Numerical Method

The hydraulic phenomena can be described by Computational fluid dynamics (CFD) techniques, where the included numerical models are solving partial differential equations of the given case. Different models are commonly used in the hydraulic studies such as the  $k-\epsilon$ ,  $k-\omega$  and Reynolds Averaged Navier-Stokes (RANS) based.

Reynolds stress models (RSM) are of high level and categorized into three types where the first one, which is the Linear Pressure-Strain model, takes the normal stress distribution near the wall into consideration, which it neglects the stress component that is tended perpendicularly to the wall. Thus, this model can be used for simple case problems. Quadratic Pressure-Strain model deals with basic shear flows which include plane strain, rotating plane shear and axisymmetric expansion/ contraction to get a superior performance. Stress-Omega model is ideal for swirling flows, since it takes modeling of flow over curved surfaces into account.

In this study, the Reynolds stress-omega model was the tool of describing the rotation of the turbines and the flow behavior around and through them, where in that model six equations are added for each time step [35]. CFD present wealthy resources for the scientific and engineering studies, especially the hydraulics [36, 37].

The Omega-RSM uses Equation (2) for  $\omega$ ; the coefficients  $\sigma$ ,  $\beta$  and  $\alpha$  are equal to 2, 0.075 and  $5/9$ , respectively.

$$\frac{\partial(\rho\omega)}{\partial t} + \frac{\partial(U_k\rho\omega)}{\partial x_k} = \alpha\rho\frac{\omega}{k}P_k + P_{\omega b} - \beta\rho\omega^2 + \frac{\partial}{\partial x_k} \left[ \left( \mu + \frac{\mu_t}{\sigma} \right) \frac{\partial\omega}{\partial x_k} \right] \quad (2)$$

where  $k$  is the turbulence kinetic energy per unit mass ( $m^2 s^{-2}$ ),  $\omega$  is the turbulent frequency ( $s^{-1}$ ),  $P_{ob}$  is the buoyancy term,  $P_k$  is the shear production of turbulence,  $\mu$  is the dynamic viscosity ( $kg m^{-1} s^{-1}$ ),  $\mu_t$  is the turbulent viscosity,  $\rho$  is the density ( $kg m^{-3}$ ). When the omega equation is included in the RSM, the dissipation tensor  $\varepsilon_{ij}$  is determined as;

$$\varepsilon_{ij} = 2/3 \delta_{ij} \beta_{RSM}^* k \omega \quad (3)$$

where  $\varepsilon_{ij}$  is a dissipation tensor,  $\delta_{ij}$  is the Kronecker delta (0 if  $i \neq j$ , 1 if  $i = j$ ), and  $\beta_{RSM}^*$  can be defined as follow:

$$\beta_{RSM}^* = \beta^* f_\beta^* \quad (4)$$

Where;

$$f_\beta^* = \begin{cases} 1 & x_k \leq 0 \\ \frac{1+680x_k^2}{1+400x_k^2} & x_k > 0 \end{cases} \quad (5)$$

$$X_k \equiv \frac{1}{\omega^3} \frac{\partial k}{\partial x_j} \frac{\partial \omega}{\partial x_j} \quad (6)$$

$$\beta^* = \beta_1^* [1 + \zeta^* F(M_t)] \quad (7)$$

$$\beta_i^* = \beta_\infty^* \left[ \frac{4 + \left(\frac{Re_t}{R_\beta}\right)^4}{15 + \left(\frac{Re_t}{R_\beta}\right)^4} \right] \quad (8)$$

$$Re_t = \frac{\rho k}{\mu \omega} \quad (9)$$

Where  $\zeta^*$ ,  $R_\beta$  and  $\beta_\infty^*$  are constants and equal to 1.5, 8 and 0.09 respectively.

#### 4. Two Dimensional Configuration

The cross-sectional shapes of both helical and straight-bladed hydrokinetic turbines are similar. The difference in the performance of the both turbines will be highlighted by 3-D numerical analyses. The cross sectional shape of the both turbines is NACA0018 hydrofoil. A 2-D simulation analysis of the selected hydrofoil was performed to clarify the general behavior. The study of the hydrodynamic characteristics of hydrofoils represents the key to understanding the performance of cross-flow turbines. The hydrofoils are designed to generate lift and most of the lift is a result of the surface pressure distribution that is consistent with Bernoulli equation;

$$p_1 - p_2 = \frac{1}{2} \cdot \rho \cdot (V_2^2 - V_1^2) \quad (10)$$

$$\therefore V_2 > V_1 \text{ and } p_2 < p_1 \quad (11)$$

The pressure distribution is expressed by a pressure coefficient,  $C_p$ . The pressure coefficient is a measure of the flow speed over the surface of the hydrofoil. High negative  $C_p$  values indicate high local velocity, relative to the free stream. When the pressure coefficient increases, an adverse pressure gradient develops. When the angle of attack (AoA) rises the minimum pressure coefficient decreases. These investigations are consequential because the rapid loss of the

lift means loss of control surface effectiveness and increment of the drag force.

A 2-D flow field behavior over NACA0018 hydrofoil with a chord of 1 m length was studied to explore the characteristics of the given foil. The analyses of flow domain around a single non-rotating hydrofoil were performed by employing the commercial code, ANSYS FLUENT. The left hand side (the outer rounded edges) boundary was set to be inflow, whereas the right side was established to be the outflow of the domain. The condition of the hydrofoil boundaries were fixed to be no-slip. The numerical model was validated at a blade Reynolds number of  $15 \times 10^5$ , which is described as follow [32]:

$$Re_{blade} = \frac{\rho v c}{\mu} \quad (12)$$

Where  $v$  and  $c$  are the incident flow velocity and the hydrofoil chord length respectively.

The initial mesh density was controlled by edge sizing. Edge sizing controls the number of divisions for each edge. This technique was implemented to increase the number of elements around the hydrofoil.

Depending on the region which is focused on, the size of the elements or the number of divisions have to be chosen after selecting the edge. Different edge sizes can be used in one flow domain when a specific region needs to be focused on. The edge size control technique was employed to get very small element sizes near the contact regions with the hydrofoil, the regions of high importance, and large element sizes at the boundaries of the fluid domain.

Generally, the hydrofoil performance is governed by the pressure distribution and forces applied on it. The drag and lift coefficients, and the pressure distribution on NACA0018 hydrofoil are examined in detail. A fluid flow past a solid body applies a force on its surface. The component of this force, which is orthogonal to the direction of flow, is called the lift force, while the other component is known as the drag force and it is parallel to flow direction. The drag force acts in the opposite direction to the object moving with respect to the surrounding fluid and it is proportional to the velocity of flow. The output power is governed by the amount of lift and drag forces, which is associated by the flowing losses [38]. Therefore, it is important to take the lift and drag resultant forces into account, as it is used to describe the performance of hydrofoils. The lift and drag forces are described by the non-dimensional lift and drag coefficients,  $C_L$  and  $C_D$ , respectively (Equations 13 and 14). The angle of attach is significantly affecting on the  $C_L$  and  $C_D$ , which influences the pressure distribution on the hydrofoil. However, the lift and drag forces are less dependent on Reynolds number [31].

$$C_L = \frac{F_L}{\frac{1}{2} \rho v^2 c A_p} \quad (13)$$

$$C_D = \frac{F_D}{\frac{1}{2} \rho v^2 c A_p} \quad (14)$$

where  $C_L$  is lift coefficient,  $C_D$  is drag coefficient,  $F_L$  is lift force (N),  $F_D$  is drag force (N),  $v$  is flow velocity ( $ms^{-1}$ ),  $c$  is the hydrofoil's chord length (m),  $A_p$  is the frontal area of blades ( $m^2$ ), equals to the chord length multiplied by the

average height of the blade (i.e. it is the projected frontal area of the blade) and  $\rho$  is fluid density ( $\text{kg m}^{-3}$ )

In order to generate the maximum power by using a cross-flow hydrokinetic turbine, the lift coefficient should be maximized while the drag coefficient needs to be minimized. Figure 2 shows a relationship between the lift coefficient and the angle of attack for NACA0018 hydrofoil, which was validated by comparing it with Ref. [27] and Ref. [39] at a single Reynolds number of  $3 \times 10^5$ . The simulation analyses exhibit almost a linear increment of the  $C_L$  up to  $8^\circ$  angle of attack. In Fig.2, the curve which shows a relationship between the AoA and the  $C_L$  seems to be composed of three parts with different slopes when a line is fitted. While in the first part the slope is the highest, in the last part the slope is the lowest. The initial variation in the slope of the curve representing the present study takes place at around  $9^\circ$  degrees angle of attack, which looks like a local jump. This phenomena occurs when the performance of the foil increases towards its optimal value at a specific angle of attack, which indicates the starting point of the stall, where the flow separation begins to increase. The occurrence of such a case may be ascribed to the onset of a hysteresis in the lift forces on the hydrofoil surface before reaching to the peak point [20]. The simulation results are in consistent with Ref. [27] and Ref. [39].

Meanwhile, the curve keeps increasing with a mild slope until it reaches the maximum lift coefficient of 1.2 at  $17^\circ$  angle of attack which is in agreement with Ref. [27], where the maximum lift coefficient obtained was about 1.22 at an angle of attack of  $17^\circ$ , while in the study of Ref. [39] a maximum lift coefficient value of 1.18 was obtained at  $15^\circ$  angle of attack. Afterwards, due to the flow separation from the surface of the foil, the results of all of the given studies demonstrate a gradual reduction in the lift coefficient and then the drag force becomes predominant. Hydrofoils with high performance enable to design efficient blades thus, turbines [24].

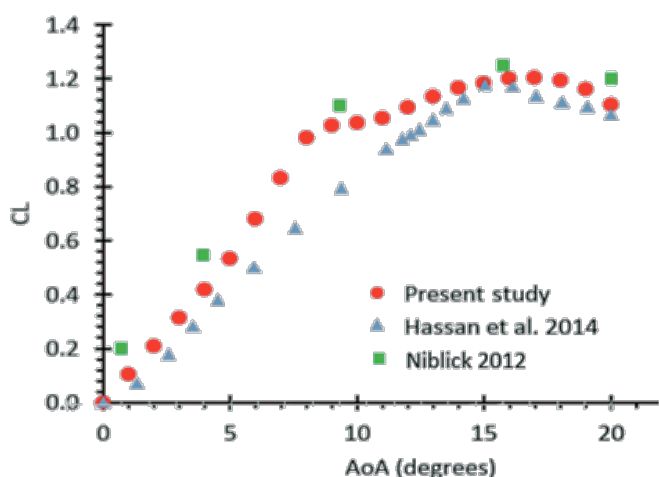


**Fig. 2.** A comparison between the predicted lift coefficient of NACA0018 and the data given by Niblic, 2012 [27] and Hassan et. al., 2014 [39] with different angles of attack at Re of  $3 \times 10^5$

The maximum lift to drag ratio was found to be achieved at  $5.5^\circ$  angle of attack for NACA0018 hydrofoil where the

curve increases rapidly until it reaches its peak value at  $5.5^\circ$  angle of attack, which gives indication about the beginning of the stall condition, and then drops gradually down to the  $10^\circ$  angle of attack, then it drops further to  $15^\circ$  angle of attack. After that the curve exhibits no significant change, meaning that the lift to drag ratio does not fluctuate considerably (Figure 3).

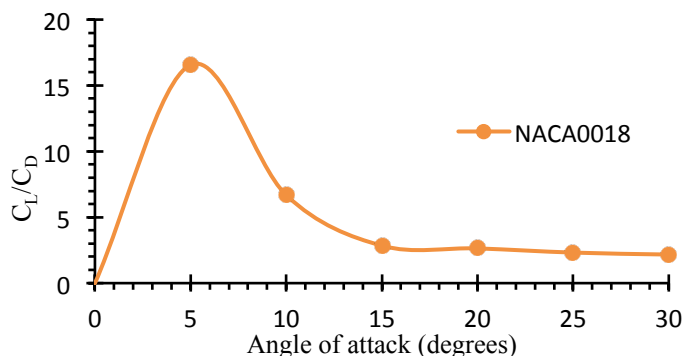


**Fig. 3.** Lift to drag ratio relationship against the angle of attack of NACA0018

The 2-D simulation results have shown that when fluid flow passes around a symmetrical hydrofoil with an angle of attack of zero degree, its surfaces will be subjected to the same pressure values, as a result, no lift force is expected to be generated (Fig.4). When the AoA increases, the upper surface of the hydrofoil will be subjected to less pressure than the lower surface, this difference in pressure produces lift forces on the hydrofoil, thus on the turbine blade (Fig.5).

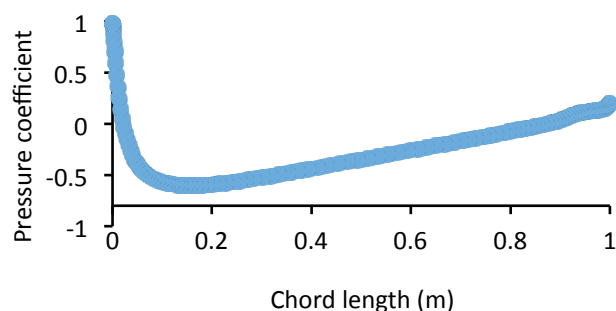


**Fig. 4.** Pressure coefficient along the upper and lower surfaces of the hydrofoil at zero degree angle of attack

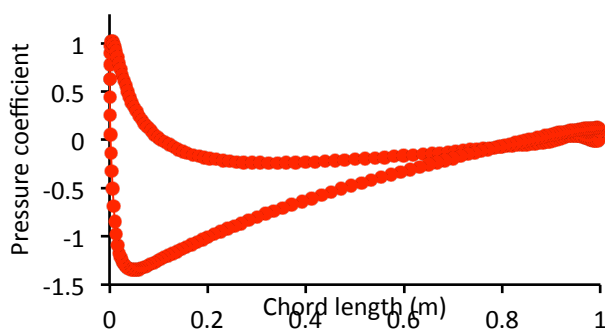


**Fig. 5.** Pressure coefficient along the upper and lower surfaces of the hydrofoil at  $5.5^\circ$  angle of attack

### 5. Three-dimensional Configuration

Unlike 2-D, 3-D model of helical and straight bladed cross flow hydrokinetic turbines differ from each other. While straight-bladed turbines have straight blades, helical turbines have twisted blades, where the twist angle in the present study was taken to be 120°. Thus, with the same turbine length, which is selected to be 1.5 m, the blade lengths of helical turbines are longer than those of straight-bladed turbines.

In order to validate the accuracy of the Reynolds stress-omega transport turbulence model, which will be employed in the simulation analyses of the present investigation, a vertical-axis two-blade helical hydrokinetic turbine is simulated with the same flow conditions and physical dimensions as in the experiments ( $Re = 2.97 \times 10^5$ ) in Ref. [21]. The helical turbine has a diameter of 0.3 m and a height of 0.45 m with two twisted blades of inclination angle of 43.68° degrees and a solidity of 0.19. Since the mesh size is expected to influence the accuracy of the simulations [40], three different mesh sizes are used in the comparative study, which are classified as coarse (148258 elements), medium (833925 elements) and fine (1462269 elements). To examine the performance of the model, the non-dimensional efficiency parameter, which is also known as the power coefficient, is considered in comparison of the simulation and the experimental results. The power coefficient ( $C_p$ ) is defined as follow [32];

$$C_p = \frac{P_t}{P_w} = \frac{T\Omega}{0.5\rho A v_{fluid}^3} \quad (15)$$

where,  $P_t$  and  $P_w$  are the turbine power output and the potential power in flowing water respectively (Watt),  $T$  is the torque to be generated (N-m),  $\Omega$  is the angular speed of the turbine ( $rad\ s^{-1}$ ),  $\rho$  is the fluid water ( $kg\ m^{-3}$ ),  $A$  is the frontal area of the turbine ( $m^2$ ) and  $v_{fluid}$  is water velocity ( $m\ s^{-1}$ ) [10, 20, 41 and 42].

The results illustrate that the simulations performed with a coarse mesh deviate from the experimental outcomes, while medium and fine meshed simulations agree well with the experimental results. The simulations underestimate the power coefficient by about a difference of 0.07 at low TSR values, while it is over estimated about a difference of 0.03 at high TSR values (Fig.6). As long as the mesh size is reasonable fine, it is possible to say that the Reynolds stress-omega transport turbulence closure model could be used in numerical analyses of hydrokinetic turbines with similar configurations in different flow conditions.

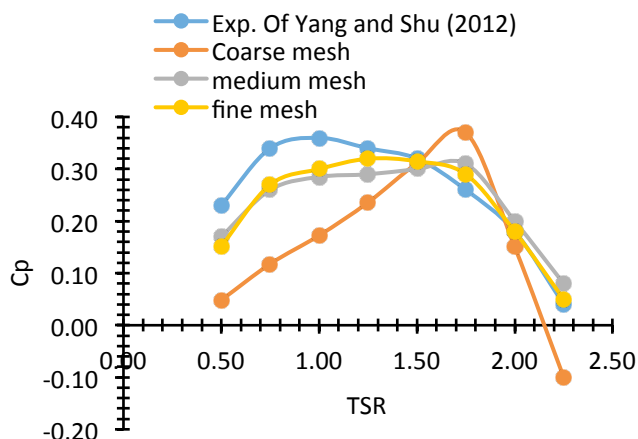


**Fig. 6.** The obtained simulation results of the power coefficient at different TSR values for the turbulence model validation study and the comparative experimental work of Yang and Shu, 2012 [21]

The 3-D simulation analyses of both helical and straight-bladed hydrokinetic turbines were performed in a semi-cylindrical channel domain with a diameter of 8 times larger than the diameter of the turbine, which is 1 m. The turbines were positioned horizontally, where the vertical distance from its center to the water surface was 1.0 m. The water surface was adjusted at 0.5 m below the top surface of the domain (Fig.7). In the present investigation, the analyses were performed at Reynolds number of  $12 \times 10^6$  and the flowing water was set to have a constant temperature of 20 C° in all simulation runs. An atmospheric pressure was given to the top of the open channel domain, the free surface.

The hydrofoil shape was based on NACA0018, the chord length was validated by the non-dimensional parameter, the solidity. Solidity is the ratio the total blade chord length to the circumference of the turbine. Blade solidity is an important design parameter for hydrokinetic turbines and it is proportional to the axial water force acting on the blades and likewise the pressure drop across the turbine. A high solidity causes flow impedance that reduces the flow velocity which passes through the turbine.

$$\sigma = \frac{b \cdot i}{2\pi R} \quad (16)$$

where  $\sigma$  is the turbine solidity,  $b$  is the chord length (m),  $i$  is the number of blades and  $R$  is the radius of the sweeping area of the turbine (m).

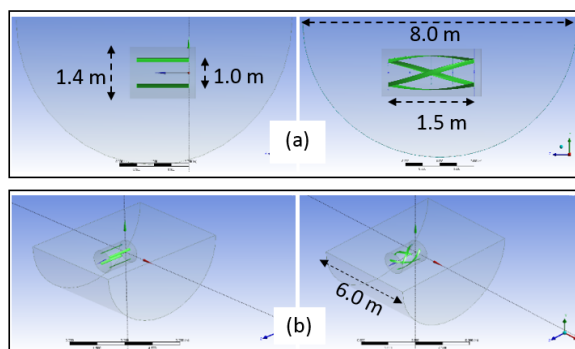


**Fig. 7.** Fluid and turbine domain for the both types: (a) front view, (b) Isometric view.

When the chord length is increased compared to the constant turbine diameter, the solidity of the turbine is also expected to be increased under the same blades number, which leads to higher resistance for the flow to pass through the turbine. This resistance depends also on the rotational speed of the turbine, if the angular velocity of the turbine keeps increasing compared to the normal flow velocity, the turbine will behave as an obstacle and the water will stop flowing through the turbine. A large amount of water will simply avoid the turbine and it will not contribute to conversion of energy, which will cause reduction in the efficiency of the turbine. The optimum solidity range of 0.3 – 0.4 is obtained by Ref. [43], and they have shown that the number of blades is associated with the solidity of the turbine. Regarding to the present study, a constant solidity value of 0.2 will be taken for the both turbines.

### 6. Mesh Quality and Solution Convergence

In computational fluid dynamics, the mesh quality effects the solution progress, thus the accuracy of the simulation results [14]. In addition, the inconsistent mesh distribution increases the calculations time or halts the whole simulation process. The total number of cells in the meshing process and their orientation with their size within the geometry are important to achieve a reasonable result. Any computational model requires a domain of interest. In the present study, the volume occupied by the fluid and a hydrokinetic turbine inside an open channel have been described by a set of computational grids, which represents a collection of small sub-domains or cells.

Both the numerical solution method and the structure of the computational grids (mesh) have significant impact on the simulation of the rotation of the turbine blades within fluid flow. Due to the expected dramatic changes in the flow field around the blades, the size of the cells should be made finer in such areas, whereas it can be left rather coarse near the open channel boundaries. Due to the complexity of the flow behavior around and within the both turbines, the cell size decreases significantly near the turbine blades, while it increases towards the outer boundaries. Since the hydrofoils and the blades are curved, an advanced curvature size function was used in the process. The curvature size function is one of the important meshing tools that is used to control the elements sizes and the curvature of edges and faces for the given geometry. The curvature size function is characterized by the limits of element size, the largest face size, the edge normal angle and the growth rate. While the curvature normal angle is expressed as the highest angle

given to the edge of the element to be spanned, the growth rate controls the length of element edges for each layer of elements

When there are regions which move relative to each other without any structural deformations, in the flow field, it is recommended to implement sliding mesh technique instead of dynamic mesh. This motion can be transitional or rotational, where it gives rise to the transient time to be used in the sliding mesh simulation [44]. In this study, the sliding mesh technique was employed to perform the meshing process for both moving and stationary zones in the flow field for the 3-D turbine models. The stationary zone, the channel domain, has the shape of a semi-cylinder with 8 m in diameter and 6 m in length, while the inner sliding cylinder, which is surrounding the turbine, has a diameter of 1.4 m.

Once the mesh is created, it must be tested and analyzed to ensure that the simulation will perform as it is expected. There are several methods which can be used to examine the accuracy of the meshing grids. Skewness is a measure used to check the quality of a mesh. It is stated that skewness ranging between 0.25 - 0.5 provides a good quality meshing [45]. The skewness was found to have a range of 0.27-0.29 of the present study, which shows that the mesh quality was quite good. In addition, the orthogonal quality test, which is performed for the meshing cells using the distance from the center of each cell to the outer faces, the face area and the distance between the centroids of the adjacent cells. The best cells have orthogonal quality values close to 1, while the worst cells have values close to zero [45]. The minimum orthogonal quality for all types of cells should be more than 0.01. Table 1 and Fig.8 clarify the reliability of the generated mesh for the given cases.

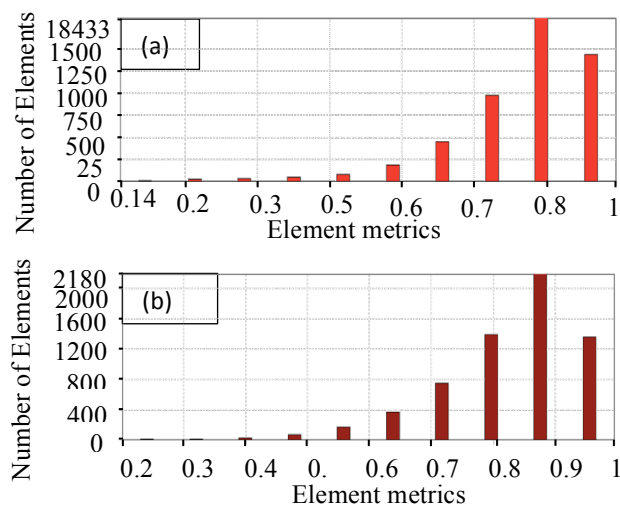


Fig. 8. Orthogonal quality of the 3-D mesh: (a) Straight-bladed turbine, (b) Helical turbine

Table 1. Mesh quality for 2-D and 3-D models

Case type	No. of nodes	No. of elements	Skewness (Avg.)	Orthogonal Quality (Avg.)
2-D hydrofoil	15912	15600	0.11	0.946
3-D turbine model (Gorlov turbine)	116900	624138	0.29	0.829
3-D turbine model (Darrieus turbine)	93065	506285	0.27	0.836

### 7. Simulations Results and Discussion

As the turbine begins to rotate, the flow velocity changes as the streamlines approaching the turbine. The enclosed domain occupied by the turbine decelerate the flow velocity and hence the pressure will be increased. Different sections have been taken upstream and downstream of the both turbines on a plane at the mid-length to get information about the flow behavior around the turbines. Figures 9 and 10 show the velocity distribution at different sections upstream and downstream of the both turbines. As the TSR value increases, the fluctuation in the velocity distribution especially at the mid length of the both turbines increases too. The velocity distribution for the both turbines showed no significant difference and this is ascribed to the same cross sectional area and azimuthal position of the blades. Because of that, the general flow pattern approximately is the same for both of them. As the water is flowing with a uniform velocity within a control volume in the absence of obstacles, the water surface remains flat, while the water level changes if the flow velocity changes due to the submerged objects, where the flow velocity becomes different in the far field domain than the surrounding one.

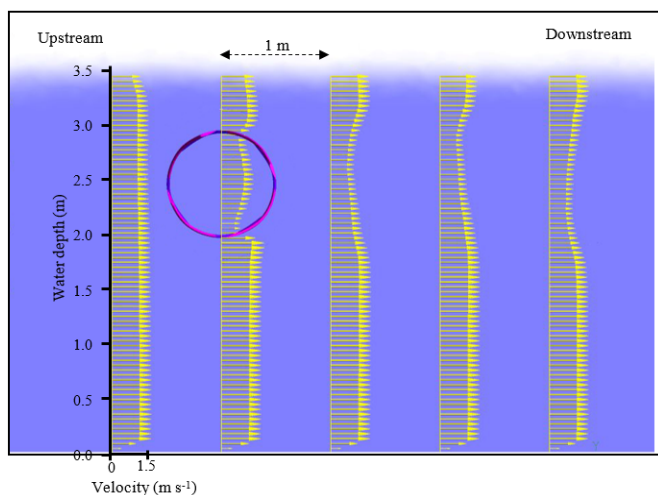


Fig. 9. Velocity profile at different sections upstream and downstream of the helical-bladed turbine

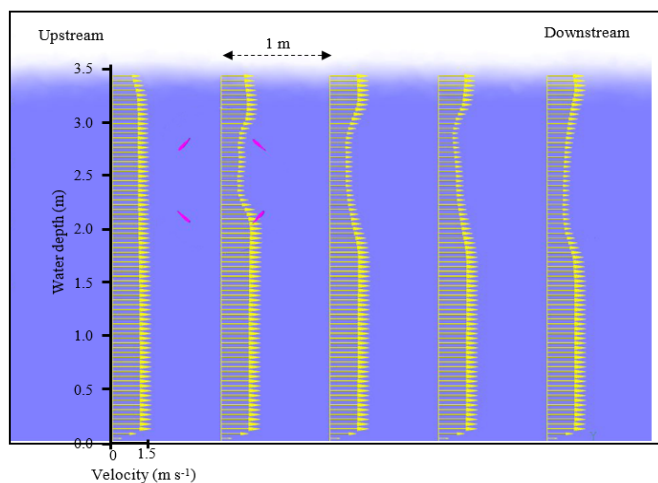


Fig. 10. Velocity profile at different sections upstream and downstream of the straight-bladed turbine

The placement of the hydrokinetic device into a channel causes resistance to the flow, resulting in reduced pressure due to the accelerated fluid. Figure 11 shows the longitudinal water surface profile for the both turbines, which is resulted in a pressure gradient. The pressure drop is manifested by the amount of water that is forced over the top of the turbine in addition to the trough created in the wake region [22, 46 – 48].

Figure 12 shows the power coefficient behavior as the angular velocity of the turbine keep increasing. It was observed that the optimum power coefficient of the helical turbine be ( $\sim 0.37$ ) at a TSR of 2.2, while the maximum power coefficient of the straight-bladed turbine was ( $\sim 0.29$ ) at a TSR of 1.9. Moreover, the straight-bladed turbine stopped harnessing energy at a TSR of about 3.1 while the helical turbine stopped producing energy at a TSR of about 3.75. The negative values of the pressure coefficient, which cause a negative torque on the blades, indicating that the turbine works normally at only a specific range of TSR, beyond that it loses its function as a turbine at high TSR values [15, 31, 49, 50 and 51].

The simulation analyses shed light on the behavior of helical and straight bladed turbines and give indication about their efficiencies under different rotational speeds, where analyses can be extended to be applied on different geometries under different flow conditions in order to get a well-designed turbine for a full-scale prototype.

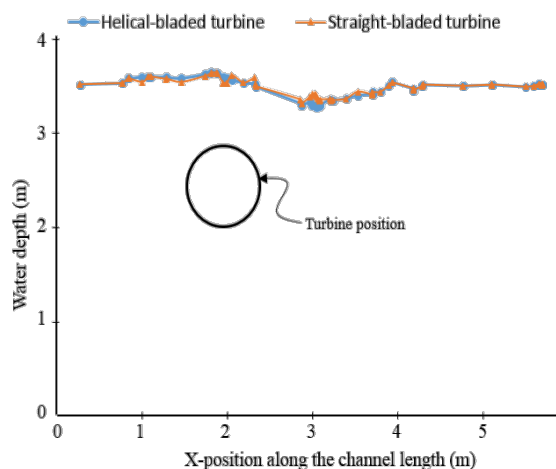


Fig. 11. Longitudinal water surface profile at the maximum performance for both turbines

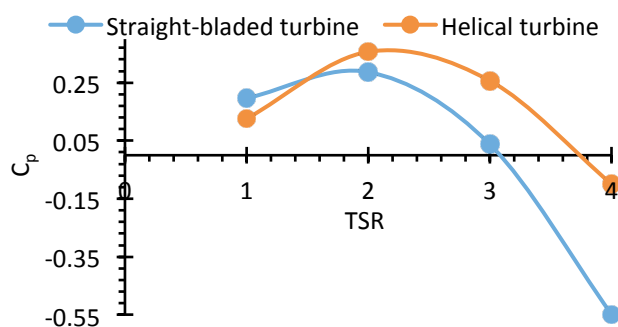


Fig. 12. The relation between power coefficient and TSR for helical and straight-bladed turbines

## 8. Conclusions

This paper presents a numerical investigation on the performance of helical and straight-bladed cross flow hydrokinetic turbines, with the same dimensions (length and diameter) and the hydrofoil type. A symmetrical NACA0018 hydrofoil was used with the solidity of 0.2 in the blade design for both turbines. The blades of the helical turbine were twisted with an angle of 120° degrees, while the blades were kept linear in the straight-bladed turbine. The simulation analyses were performed for a 2-D NACA0018 hydrofoil and 3-D four bladed turbines of helical and straight-bladed shapes. The dimensions of the turbines were chosen to be the same, 1.5 m in length and 1 m in diameter. Different parameters, such as, Reynolds number, tip-speed-ratio (TSR), solidity and power coefficient were considered to identify the flow field through and around the turbines.

The simulation analyses of the hydrofoil provide evidence that at 0° degree angle of attack, the pressure distribution is the same on the upper and lower surfaces of the foil, thus, there is no lift on the hydrofoil. When the angle of attack increases up to around 9° degrees, the lift coefficient increases linearly, then a hysteresis occurs in the lift due to the beginning of flow separation. The lift coefficient keeps increasing as the angle of attack increases further with a milder slope until it reaches its maximum value.

Moreover, the results of the 3-D simulations have shown that the helical turbine reaches the stall condition at the TSR of about 3.75, while the straight-bladed turbine stops converting energy at the TSR of about 3.1. Since the turbines act as obstacles, which create a resistance to water flow causing a pressure gradient across the turbines indicating a change in water surface elevation. The maximum power coefficient that obtained for the helical turbine was 0.37 at the TSR of 2.2, while it was 0.29 at the TSR of 1.9 for the straight-bladed turbine. Nevertheless, the helical turbine was found to be more efficient than the same-sized straight-bladed turbine under the same flow conditions, the flow field around both turbines was approximately the same. This can be attributed to the similarity in cross sectional area of the turbines. The aforementioned investigations and the related results make several noteworthy contributions in designing hydrokinetic turbines with different geometries in order to obtain the maximum performance.

## References

- [1] M. Mueller, R. Lopez, A. McDonald and G. Jimmy, "Reliability analysis of wave energy converters", *Renewable Energy Research and Applications (ICRERA), IEEE International Conference*, Birmingham, UK, DOI: 10.1109/ICRERA.2016.7884418, 2016.
- [2] E. Aydin, A. Polat and L. T. Ergene, "Vector control of DFIG in wind power applications", *Renewable Energy Research and Applications (ICRERA), IEEE International Conference*, Birmingham, UK, DOI: 10.1109/ICRERA.2016.7884383, 2016.
- [3] O. Kaplan and M. Temiz, "The analysis of wind speed potential and energy density in Ankara", *Renewable Energy Research and Applications (ICRERA), IEEE International Conference*, Birmingham, UK, DOI: 10.1109/ICRERA.2016.7884469, 2016.
- [4] M. Abdollahi, J. L. Candela, J. Rocabert, R. S. M. Aguilar and J. R. Hermoso, "Synchronous power controller merits for dynamic stability improvement in long line by renewables", *Renewable Energy Research and Applications (ICRERA), IEEE International Conference*, Birmingham, UK, DOI: 10.1109/ICRERA.2016.7884438, 2016.
- [5] S. Demirbas, R. Bayindir, A. Ova, U. Cetinkaya and M. Yesil, "Stability analysis of an offshore wind farm connected to turkish electricity transmission system", *Renewable Energy Research and Applications (ICRERA), IEEE International Conference*, Birmingham, UK, DOI: 10.1109/ICRERA.2016.7884558, 2016.
- [6] K. D. Mercado, J. Jiménez, M. Christian and G. Quintero, "Hybrid renewable energy system based on intelligent optimization techniques", *Renewable Energy Research and Applications (ICRERA), IEEE International Conference*, Birmingham, UK, DOI: 10.1109/ICRERA.2016.7884417, 2016.
- [7] O. V. Marchenko and S. V. Solomin, "Efficiency of Hybrid Renewable Energy Systems in Russia", *International Journal of Renewable Energy Research IJRER*, Vol.7, No.4, 2017.
- [8] K. Kajiwara, S. Kuboyama, T. Higuchi, J. W. Kolar and F. Kurokawa, "A new digital current control AC-DC converter for wind turbine", *Renewable Energy Research and Applications (ICRERA), IEEE International Conference*, Birmingham, UK, DOI: 10.1109/ICRERA.2016.7884429, 2016.
- [9] N. Mehmood, Z. Liang, and J. Khan, "Harnessing Ocean Energy by Tidal Current Technologies", *Research Journal of Applied Sciences, Engineering and Technology*, Vol. 4, No. 18, pp. 3476-3487, 2012.
- [10] M. I. Yuce and A. Muratoglu, "Hydrokinetic energy conversion systems: A technology status review", *Renewable and Sustainable Energy Reviews*, Doi: 10.1016/j.rser.2014.10.037, Vol. 43, pp. 72–82, 2015.
- [11] D. S. Semerci and T. Yavuz, "Increasing efficiency of an existing francis turbine by rehabilitation process", *Renewable Energy Research and Applications (ICRERA), IEEE International Conference*, Birmingham, UK, DOI: 10.1109/ICRERA.2016.7884440, 2016.
- [12] S. M. Braun and M. Burkhardt, "Trading of pumped storage hydropower plants on energy only and ancillary services markets", *Renewable Energy Research and Applications (ICRERA), IEEE International Conference*, Palermo, Italy, DOI: 10.1109/ICRERA.2015.7418492, 2015.
- [13] A. Gorlov, "Development of the helical reaction hydraulic turbine", *Final Technical Report*, 1998.

- <https://digital.library.unt.edu/ark:/67531/metadc707246/m1/> (accessed on 13 June 2017)
- [14] Y. C. Ceballos, M. C. Valencia, D. H. Zuluaga, J. S. Del Rio and S. V. García, "Influence of the Number of Blades in the Power Generated by a Michell Banki Turbine", *International Journal Of Renewable Energy Research IJRER*, Vol. 7, No. 4, 2017
- [15] C. A. Consul, R. H. Willden, E. Ferrer and M. D. McCulloch, "Influence of Solidity on the Performance of a Cross-Flow Turbine", *Proceedings of the 8th European Wave and Tidal Energy Conference*, Uppsala, Sweden, 2009.
- [16] M. Karimirad and K. Koushan, "WindWEC: Combining wind and wave energy inspired by hywind and wavestar", *Renewable Energy Research and Applications (ICRERA)*, IEEE International Conference, Birmingham, UK, DOI: 10.1109/ICRERA.2016.7884433, 2016.
- [17] S. Schwartz, and K. Argyiadis, "Certification of ocean current turbines", *The 6th European Wave and Tidal Energy Conference*, Glasgow, UK, 2005.
- [18] A. KATKOUT, A. ESSADKI and T. NASSER, "Nonlinear Power Control Strategies for Variable- Speed Wind Turbines", *International Journal of Renewable Energy Research IJRER*, Vol. 7, No. 4, 2017.
- [19] A.S.O. Ogunjuyigbe, T.R. Ayodele, B. B. Adetokun and A.A. Jimoh, "Dynamic performance of wind-driven self-excited reluctance generator under varying wind speed and load", *Renewable Energy Research and Applications (ICRERA)*, IEEE International Conference, Birmingham, UK, DOI: 10.1109/ICRERA.2016.7884388, 2016.
- [20] R. McAdam, *Studies into the Technical Feasibility of the Transverse Horizontal Axis Water Turbine*, PhD Thesis, Keble College, University of Oxford, 2011.
- [21] B. N. Yang, and X. W. Shu, "Hydrofoil optimization and experimental validation in helical vertical axis turbine for power generation from marine current", *Journal of Ocean Engineering*, Vol. 42, pp. 35 - 46, 2012.
- [22] M. G. Gebreslassie, G. R. Tabor and M. R. Belmont, "Numerical simulation of a new type of cross flow tidal turbine using Open FOAM-Part II: Investigation of turbine-to-turbine interaction", *Journal of Renewable Energy*, Vol. 50, pp. 1005-1013, 2013.
- [23] Y. M. Dai, N. Gardiner, R. Sutton and P. K. Dyson, "Hydrodynamic analysis models for the design of Darrieus-type vertical-axis marine current turbines. Part M", *Journal of Engineering for the Maritime Environment*, Vol. 225, pp. 295-307, 2011.
- [24] F. Javed, S. Javed, T. Bilal and V. Rastogi, "Design of multiple airfoil HAWT blade using MATLAB programming", *Renewable Energy Research and Applications (ICRERA)*, IEEE International Conference, Birmingham, UK, DOI: 10.1109/ICRERA.2016.7884373, 2016.
- [25] H. Cao, *Aerodynamics Analysis of Small Horizontal Axis Wind Turbine Blades by Using 2D and 3D CFD Modelling*, MSc. Thesis, University of the Central Lancashire, Preston, England, 2011.
- [26] J. Winchester, and S. Quayle, "Torque ripple and power in a variable pitch vertical axis tidal turbine", *The 9th European Wave and Tidal Energy Conference*, Southampton, UK, 2011.
- [27] A. L. Niblick, *Experimental and Analytical Study of Helical Cross-Flow Turbines for a Tidal Micro power Generation System*, MSc. Thesis, University of Washington, 2012.
- [28] K. Syed Shah, Z. Liang, and N. Shah, "Harnessing Tidal Energy Using Vertical Axis Tidal Turbine", *Research Journal of Applied Sciences, Engineering and Technology*, Vol. 5, No. 1, pp. 239-252, 2013.
- [29] A. Zingman, *Optimization of a Savonius Rotor vertical-axis wind turbine for use in water pumping systems in rural Honduras*, B.Sc. project, M.I.T., USA, 2007.
- [30] J. Anderson, B. Hughes, C. Johnson, N. Stelzenmuller, L. Sutanto, B. Taylor, A. Niblick and E. McQuaide, *Design and Manufacture of a Cross-Flow Helical Tidal Turbine*, Capstone Project Report, the University of Washington, 2011,  
<[http://depts.washington.edu/nnmrec/docs/20110615\\_ME495\\_report\\_Micropower.pdf](http://depts.washington.edu/nnmrec/docs/20110615_ME495_report_Micropower.pdf)> (accessed on 13 June 2017)
- [31] R. A. McAdam, G. T. Houlsby, M. L. G. Oldfield, and M. D. McCulloch, "Experimental Testing of the Transverse Horizontal Axis Water Turbine", *Proceedings of the 8th European Wave and Tidal Energy Conference*, Uppsala, Sweden, 2009.
- [32] A. Benzerdjeb, B. Abed, M. K. Hamidou, M. Bordjane and A. M. Gorlov, "Experimental Study on the Effect of Water Velocity on the Performance of a Cross-Flow Turbine", *International Journal of Renewable Energy Research IJRER*, Vol. 7, No. 4, 2017.
- [33] A. Al-Sam, *Water wheel CFD simulations*, MSc thesis, Lund University, Sweden, 2010.
- [34] S. L. Dixon, *Fluid Mechanics and Thermodynamics of Turbo Machinery*. 5th ed. Elsevier Butterworth-Heinemann, 1998.
- [35] C. G. Speziale, S. Sarkar, and T. B. Gatski, "Modeling the Pressure-Strain Correlation of Turbulence: An Invariant Dynamical Systems Approach", *J. of Fluid Mechanics*, Vol. 227, pp. 245-272, 1991.
- [36] C. Biscarini, S. D. Francesco, and P. Manciola, "CFD modelling approach for dam break flow studies", *Hydrol. Earth Syst. Sci*, Vol. 14, pp. 705-718, 2010.
- [37] G. Chevallet, M. Jellouli, and L. Deroo, "Democratization of 3D CFD hydraulic models: several Examples performed with ANSYS CFX", *SimHydro: New trends in simulation*. Sophia Antipolis, 2012.

- [38] O. Günel, E. Koç and T. Yavuz, "CFD vs. XFOIL of airfoil analysis at low Reynolds numbers", Renewable Energy Research and Applications (ICRERA), IEEE International Conference, Birmingham, UK, DOI: 10.1109/ICRERA.2016.7884411, 2016.
- [39] G. E. Hassan, A. Hassan and M. E. Youssef, "Numerical investigation of medium range Reynolds number aerodynamics characteristics for NACA0018 airfoil", CFD Letters, 6(4), 2014.
- [40] S. R. Turnock, A. B. Phillips, J. Banks and R. N. Lee, "Modelling tidal current turbine wakes using a coupled RANS-BEMT approach as a tool for analyzing power capture of arrays of turbines", Journal of Ocean Engineering, <http://dx.doi.org/10.1016/j.oceaneng.2011.05.018>, Vol. 38, pp. 1300-1307, 2011.
- [41] A. N. Gorban, A. M. Gorlov, and V. M. Silantyev, "Limits of the Turbine Efficiency for Free Fluid Flow", Journal of Energy Resources Technology, ASME, Vol. 123, pp. 311-317, 2001.
- [42] A. Chesna, T. Di Bella, T. Hutchins, S. Kropf, J. Lesica, and J. Mahoney, Hydroelectric power generator. Capstone Design Program, department of Mechanical Engineering, Northeastern University, 2007, [https://repository.library.northeastern.edu/downloads/neu:377527?datastream\\_id=content](https://repository.library.northeastern.edu/downloads/neu:377527?datastream_id=content) (accessed on 13 June 2017)
- [43] M. Shiono, K. Suzuki, and S. Kiho, "Output Characteristics of Darrieus Water Turbine with Helical Blades for Tidal Current Generators", Proceedings of the 12th International Offshore and Polar Engineering Conference, Kitakyushu, Japan, 2002.
- [44] J. McNaughton, D. Afgan, D. Apsley, S. Rolfo, T. Stallard, and P. Stansby, "A simple sliding-mesh interface procedure and its application to the CFD simulation of tidal-stream turbine", International journal for numerical methods in fluids, Vol. 74, pp. 250-269, 2013.
- [45] ANSYS 14.5 Meshing User's Guide.
- [46] A. H. Chime, Analysis of Hydrokinetic Turbines in Open Channel Flows, MSc. Thesis, University of Washington, 2013.
- [47] A. H. Chime and P. C. Malte, "Hydrokinetic turbines at high blockage ratio", Proceedings of the 2nd Marine Energy Technology Symposium METS, Seattle, WA, 2014.
- [48] B. Kirke and L. Lazauskas, "Variable Pitch Darrieus Water Turbines", Journal of fluid science and technology, DOI: 10.1299/jfst.3.430, Vol. 3, No. 3, 2008
- [49] S. R. Helms, Simulation of vertical axis wind turbine blades, M.Sc. Thesis, department of Mechanical Engineering, University of Drexel, 2011.
- [50] J. McNaughton, Turbulence modelling in the near-field of an axial flow tidal turbine using code-saturne, PhD Thesis, School of Mechanical, Aerospace & Civil Engineering, University of Manchester, 2013.
- [51] M. A. AL-DABBAGH, Simulation of Helical Hydrokinetic Turbines in River Flows, PhD Thesis, Department of Civil Engineering, University of Gaziantep, Turkey, 2017.